

Improving Zero-Shot Object-Level Change Detection by Incorporating Visual Correspondence

Hung H. Nguyen

Auburn University

hhn0008@auburn.edu

Pooyan Rahmanzadehgervi

Auburn University

pooyan.rmz@gmail.com

Long Mai

Adobe Research

mai.t.long88@gmail.com

Anh Totti Nguyen

Auburn University

anh.ng8@gmail.com



Figure 1. At an optimal confidence threshold, CYWS [25] (top row) sometimes still produces false positives— \square in (a) & (c)—and fails to detect changes (a). Dashed $---$ boxes show groundtruth changes. First, we encourage detectors to be more aware of changes via a novel contrastive loss. Second, our Hungarian-based post-processing reduces false positives (a), improves change-detection accuracy (b), and estimates correspondences (c–d), i.e., paired changes such as (\square, \square) and (\square, \square) . Our work (bottom row) is *the first* to estimate change correspondences compared to prior works [25, 26, 40] (top row). More qualitative results in (Fig. A4).

Abstract

Detecting object-level changes between two images across possibly different views (Fig. 1) is a core task in many applications that involve visual inspection or camera surveillance. Existing change-detection approaches suffer from three major limitations: (1) lack of evaluation on image pairs that contain no changes, leading to unreported false positive rates; (2) lack of correspondences (i.e., localizing the regions before and after a change); and (3) poor zero-shot generalization across different domains. To address these issues, we introduce a novel method that leverages change correspondences (a) during training to improve change detection accuracy, and (b) at test time, to minimize false positives. That is, we harness the supervision labels of where an object is added or removed to supervise change detectors, improving their accuracy over previous work [25] by a large margin. Our work is also the first to predict correspondences between pairs of detected changes using estimated homography and the Hungarian algorithm. Our model demonstrates superior performance over existing methods, achieving state-of-the-art results in change detection and change correspondence accuracy across both

in-distribution and zero-shot benchmarks.

1. Introduction

Identifying key changes between two images is a core task that powers many applications [25], e.g., to detect changes across brain scans [6, 22], a missing car in a parking lot (Fig. 1) [13, 31], or a defective product in a manufacturing pipeline [36]. However, existing work has three major limitations. First, most papers did not test on pairs of images where there are no changes [25, 26] and therefore do not measure false positives. Many image-difference captioning benchmarks contain only *change* cases [34] or only a small subset of *no-change* examples, e.g., 10% of Spot-the-Diff [13]. Second, prior models are trained to detect only changes; yet, such detected changes are not too usable in the downstream application when there are many changes predicted per image but no correspondence provided (Fig. 1). Third, many image-difference prediction works are specialized for a single domain (e.g., remote sensing [37]) and do not measure zero-shot generalization to unseen datasets [37, 40].

In this paper, we address these three problems by leveraging change correspondences during (a) training to improve change detection precision, and (b) test time to reduce false positives. Compared to prior works [25, 26, 40], **our work is the first to predict correspondences in addition to the changes** (Fig. 1). That is, we propose a post-processing algorithm based on an estimated homography and the Hungarian algorithm [2, 17] to reduce false positives (Fig. 1) of a state-of-the-art change detector [25]. Intuitively, first, we run a pre-trained change detector [25] on a pair of images to collect a set of predicted changes on each image. Then, we project the predicted boxes in image 1 onto image 2 and filter out those that do not substantially overlap with any predicted changes in image 2, arriving at higher-precision change predictions (Fig. 4). A similar procedure is used to filter out the predicted changes in image 2. We then harness the Hungarian algorithm to predict correspondences in addition to the predicted changes (Fig. 1). Our main findings are:¹

1. Leveraging correspondence labels in finetuning detectors leads to state-of-the-art change detectors, outperforming CYWS [25] by a large margin (from +1.05 to +9.04 in mAP) on all five benchmarks (Sec. 5.1).
2. Our proposed contrastive matching loss function for finetuning change detectors also improves the accuracy in predicting correspondences, from +1.31 to +6.56, on all five benchmarks (Sec. 5.2).
3. Moreover, we have established a new metric for evaluating matching scores among different models, facilitating a consistent and comparative assessment of change detection performance (Sec. 2.3).
4. We present OpenImages-Inpainted, *i.e.*, a novel change detection dataset with $\sim 1.3\text{M}$ image pairs, where image pairs consist of exactly 1 change derived from realistic scenes of the OpenImages [18] dataset. Our OpenImages-Inpainted has no view-transformation artifacts (compared to COCO-Inpainted [25]) and minimal inpainting artifacts (compared to Img-Diff [14]).

2. Problem formulation

2.1. Definition of Changes


We define a change to be an addition, absence, or modification of an **object** in one image compared to the other (see Fig. 2a–b). A major challenge is to detect such object-level changes in the presence of changes in camera viewpoint (COCO-I, KC), colors (COCO-I), or lighting (STD), which we do not aim to detect. The objects that change include


humans, animals (COCO-I), man-made objects (COCO-I, STD, KC, OI), and letters (SC).


In the case where the same object *moves* from one location to another (Fig. 2c) across two images, we expect two changes to be detected: (1) An object is removed from the first location in image 1, and (2) an object is added to the second location in image 2. That is, two pairs of corresponding changes are to be predicted.


2.2. Five benchmarks



Following [25], we train and test both our model and CYWS [25] on COCO-Inpainted. Additionally, we test these models **zero-shot** on four *unseen* change-detection benchmarks: STD [13], Kubric-Change [25], and Synthtext-Change [25] and our proposed OpenImages-Inpainted.

COCO-Inpainted (COCO-I)  [25] contains 57K, 3K, and 4.5K image pairs in the train, validation, and test sets, respectively. In each pair, one image is originally from COCO and the other is a clone with N objects removed ($1 \leq N \leq 24$) from the image. The test set is divided into three groups based on the size of removed objects: small (38%), medium (39%), and large (23%) (see Fig. 2a). Images are subjected to random affine transformations and color jittering. Combined with cropping, these modifications yield image pairs, where all objects may not appear in both images.

VIRAT-STD (STD)  [13] A random 1,000 pairs of images (see Fig. 2b) is selected from the Spot-the-Difference dataset [13], a dataset of camera surveillance images of street views. Two images in each pair have almost identical views but are taken at different times. Objects being changed are typically humans and cars.

Kubric-Change (KC)  [25] comprises 1,605 test cases (see Fig. 2c). The scenes comprise a randomly chosen assortment of 3D objects on a ground plane with a random texture. After applying the change to the scene, the camera’s position in the 3D space slightly moves, yielding two different views of the scene.

Synthtext-Change (SC)  [25] consists of 5K pairs of real images with N changes, where $1 \leq N \leq 6$. Each change includes an arbitrary letter synthetically placed on one image at random locations.

OpenImages-Inpainted (OI)  To address the view-transformation and inpainting artifacts in  and Img-Diff [14], we create $\sim 1.3\text{M}$ pairs of images containing exactly 1 change. We adopt the original images from OpenImages dataset [18], and remove a single object using LaMa [33] inpainter, similar to COCO-I [25]. We filter the object sizes based on their relative bounding box area to the image size and keep the objects that fall within the range of 0.01 to 0.04. This ensures that objects are neither tiny nor overly large. We rotate a random image in the pair within the range of $[-10, 10]$ degrees, and then apply random croppings to

¹Code and data are available on [github](https://github.com).

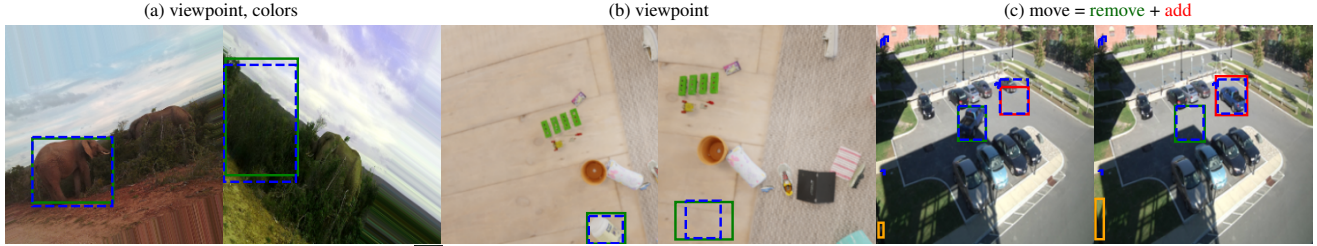


Figure 2. **Example predicted changes.** In (a), our method detects a removal of an elephant (a) despite viewpoint and color differences between two images. A tiny, white object (b) removal is detected despite viewpoint differences in (b). In (c), a blue truck moving from one location to another is correctly detected as two changes: a removal and an addition. Colored, solid-bordered boxes, e.g., (red box), (blue box), (green box), (red box), (blue box), show predicted *paired* changes.

generate viewpoint differences. We use a 5K subset for testing and the remaining images for training.

2.3. Evaluation metrics

Change detection evaluation We use object localization metrics to evaluate the accuracy of change detection. Specifically, we follow CYWS and use mAP for the top $k = 100$ predicted boxes with the highest confidence scores in PASCAL VOC [20] style (see the code). We threshold bounding boxes by confidence scores to filter out low-confidence predictions, ensuring better precision by reducing the false positives (FP) for mAP.

Correspondence evaluation Common metrics for change detection focus on detecting changed objects, ignoring the correspondence information [25, 26]. We are the first to adopt the F1 score ($\frac{2 \times \text{Precision} \times \text{Recall}}{\text{Precision} + \text{Recall}}$) from the classification tasks to evaluate the correctness of the correspondence predictions in the change detection task. That is, we compare each predicted pair of correspondence to the ground truth corresponding boxes to see if they match.

We define True Positive (TP), False Positive (FP), and False Negative (FN):

- **TP:** For each predicted box in the correspondence pair, we calculate their IoU with ground truth. If the IoU value for each predicted box in the pair is ≥ 0.5 , the pair is labeled TP. If more than 1 prediction matches the same ground truth, the pair with the highest IoU value, for each box in the pair, is assigned TP.
- **FP:** Any predicted pair in which either one or both of its boxes does not meet the $\text{IoU} \geq 0.5$ criteria is labeled FP. If the boxes in the pair meet the criteria but do not have the highest IoU, we label them FP.
- **FN:** For each ground truth box, if there is no predicted pair with a nonzero IoU, we label the prediction FN.

3. Methods

CYWS [25], a SOTA change detection model, is a U-Net coupled with CenterNet head [7] to detect changes in two

images. That is, they predict 100 boxes per image, assuming the images always contain changes. Here, we summarize the current problems with this method that limit its real-world applications.

1. They assume that each image pair always contains ≥ 1 changes. However, there are many cases in the real world where no changes exist.
2. Given that they only detect boxes and the correspondence information is not predicted, it is not trivial to understand and relate its predictions with each other across two images when several changes are present (see Fig. 1).

In this work, we aim to solve these problems, *i.e.*, we address both **change** and **no-change** scenarios and predict a correspondence between the changed objects.

Our change detection pipeline consists of 3 stages: (1) change detection backbone, (2) alignment, and (3) correspondence prediction. Given a pair of images in Stage 1 (Fig. 3), a change detector *e.g.*, CYWS [25], detects boxes over the changed objects. Then, in Stage 2, we aim to reduce the false positive predictions and remove the boxes that are poor candidates for correspondence prediction via an alignment stage. Finally, we use the Hungarian algorithm with a contrastive matching loss to predict the correspondences in Stage 3.

3.1. Stage 1: Change detection

The change detection backbone identifies change locations between left and right images using bounding boxes. After applying an optimal detection threshold to filter out predicted boxes with low confidence scores, the remaining bounding boxes are used as input for Stage Two and Stage Three (Fig. 3).

U-Net encoder The ResNet-50 architecture is employed as the encoder backbone. The input image has a shape of $3 \times 256 \times 256$. The output of the last layer (Layer 4.2) has a shape of $8 \times 8 \times 2048$.

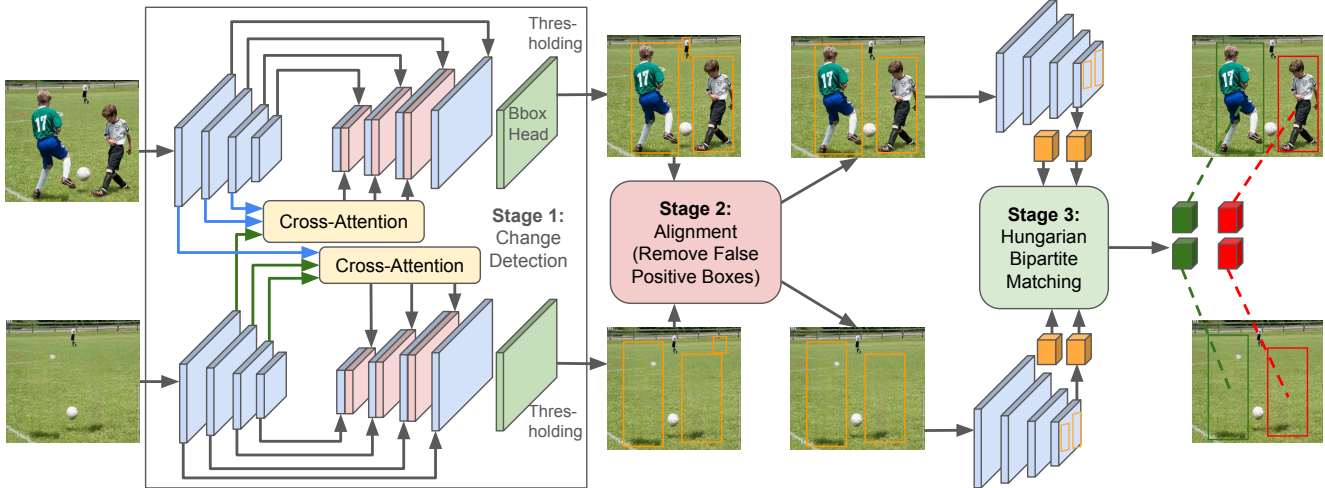


Figure 3. **Our approach of detecting changes and predicting their correspondence.** Our approach comprises three major stages. The first is the change detector, which we employ from the CYWS paper to identify changes between two images. The second is the alignment step, where an ideal detection threshold is established before forwarding anticipated boxes to the alignment process, aiding in the removal of false positive predicted boxes. The third is the matching algorithm, which takes the output from the alignment step to determine the correspondence between each pair of changes between the two images.

Cross-attention The cross-attention module facilitates information exchange between left and right images, enabling accurate computation of changes between the two. This process generates three feature maps with shapes $8 \times 8 \times 4096$, $16 \times 16 \times 2048$, and $32 \times 32 \times 1024$, respectively.

U-Net decoder The decoder utilizes the three feature maps produced by the cross-attention module as input and up-samples them to generate feature maps with a shape of $64 \times 256 \times 256$. Skip connections from the encoder and scSE [24] blocks are incorporated into the upsampling process. The decoder output passes to the Bbox head.

Bbox head: The bbox head employs CenterNet [7] to predict bounding boxes for the detected change regions in the two images. CenterNet produces three output maps: center map ($1 \times 256 \times 256$), offset map ($1 \times 256 \times 256$), and height-width map ($2 \times 256 \times 256$).

3.2. Stage 2: Alignment

Thresholding the box predictions with the confidence score significantly reduces the number of false positives (Tab. 6). However, we take an additional step to eliminate boxes that are poor candidates for alignment. The alignment stage is based on the premise that if a predicted change box appears in the left image, there should be a corresponding box in the right image. This helps us refine candidate boxes for the subsequent matching stage in our proposed solution.

To identify the alignment box of a candidate box in the left image, we first determine the transformation matrix—an affine transformation between the two images. We use SuperGlue [29] to establish point correspondences between the images, and apply RANSAC to eliminate outliers. We

use SuperGlue because of its lightweight and high accuracy point-matching performance [29].

A candidate box is valid if its alignment overlaps with any box in the other image ($\text{IoU} > 0$). Otherwise, it is invalid and excluded. Two candidate boxes (red and green) in the left image are aligned with corresponding dashed boxes in the right image. The red box’s alignment overlaps with the orange box, making it valid, while the green box’s alignment does not overlap and is discarded (Fig. 4b).

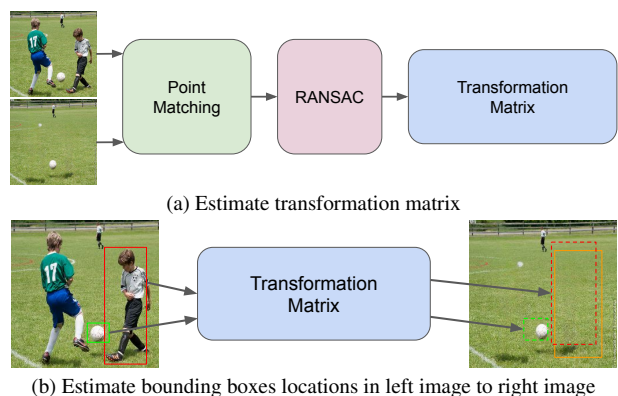


Figure 4. **Alignment Overview.** (Fig. 4a) illustrates the process for estimating the homography matrix. In (Fig. 4b), dashed \square represent the corresponding box in the right image of \square in the left image. Similarly for \square box.

3.3. Stage 3: Correspondence prediction

The alignment stage combined with the confidence thresholding substantially reduces the false positives, yielding improved mAP on five benchmarks (see Tab. 3). Yet, the lack of correspondence information remains unsolved (see the outputs of Stage 2 in Fig. 3).

Here, we aim to predict the correspondence between the predicted boxes for each image pair given the embeddings of each box. That is, we first extract embeddings from the feature maps in the backbone (Stage 1) for each aligned box of Stage 2. Then, we use the Hungarian bipartite matching algorithm jointly with a contrastive matching loss to predict the final correspondence.

Box embedding extraction Since each predicted box intersects with ≥ 1 image patches in the feature maps of Stage 1, we use 2 different methods to extract the box embeddings, and choose the best one based on the mAP score in App. B:

1. **Mean pooling Method:** We hypothesize that the mean of patches associated with a predicted box enriches the correspondence embedding vector of the box with contextual information surrounding the object. We input each image (of size 256×256) into the image encoder to obtain a feature volume of $8 \times 8 \times 2048$. From the $8 \times 8 = 64$ patch embeddings, we select all N embeddings corresponding the patches that overlap with a given bounding box in the input image space. Then, we take the mean of the N embeddings to obtain final embedding of size 2048 (code).
2. **Region Cropping Method:** This method evaluates whether excessive contextual information surrounding an object negatively impacts the quality of the embedding vector. To address this, only the information within the predicted bounding box is utilized. We crop the input image to bounding-box region to create a cropped image (code). We feed the cropped image into a ResNet-50 image encoder and average the $8 \times 8 \times 2048$ feature output from layer 4.2 to obtain a 2048 dimensional embedding.

A key challenge in implementing change detection in real-world scenarios is identifying the correspondence between changes detected in two images. We use the Hungarian algorithm to match the predicted bounding boxes between the two images. Given, e_i , and e_j , the embeddings of two bounding boxes from (Sec. 3.3) we calculate a cost matrix using the ground distance (Eq. (1)) similar to [23].

$$d_{ij} = 1 - \frac{\langle e_i \cdot e_j \rangle}{\|e_i\| \|e_j\|} \quad (1)$$

where i, j are indices of matrix elements. Using the cost matrix the Hungarian algorithm assigns the correspondence

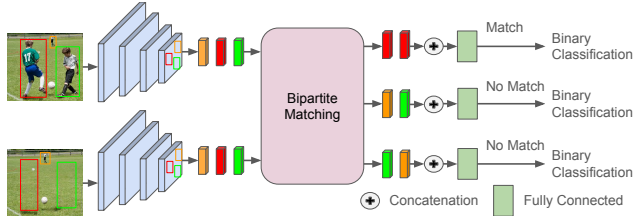



Figure 5. **Contrastive matching loss.** Contrastive matching loss trains the model to distinguish between positive and negative pairs of image patches. Each ground-truth bounding box is assigned an embedding from the last layer of encoder, and the Hungarian algorithm is employed to establish matches between ground-truth boxes across two images. A matched pair is labeled as positive if it aligns with the correspondence ground truth; otherwise, it is designated as negative. Embeddings of positive and negative pairs are concatenated and passed through a fully connected layer to compute BCELoss.

between boxes from the first and second image such that the total cost is minimum.

Contrastive matching loss We use the contrastive matching loss to train the model to classify pairs of matched boxes obtained from the Hungarian algorithm. The Hungarian algorithm is not perfectly accurate, *i.e.*, it achieves an F1 score of 91.68% on the  dataset (see App. A) when using the ground truth boxes, and it generates both negative and positive matchings. Specifically, we compare the matched boxes with the correspondence information in the ground truth, classifying them as either: (1) positives, *i.e.*, they match the ground truth, or (2) negatives, *i.e.*, they do not. We leverage this fact and train the model using our contrastive matching loss. First, the embeddings of matched pairs are concatenated and processed through a fully connected layer. Then, we use a binary classification loss (BCELoss), treating the matched pairs as predictions and the ground-truth correspondence as targets.

The final training objective in (Eq. (2)) consists of two main components: (1) object detection loss and (2) contrastive matching loss. The detection loss integrates center-based loss components, ensuring precise localization and classification.

$$L_{\text{total}} = L_{\text{CenterNet}} + \alpha L_{\text{DETR}} + \beta L_{\text{contrastive}} \quad (2)$$

where $L_{\text{CenterNet}}$ is the CenterNet detection loss [7], and L_{DETR} [2] is the combination of L_1 loss and GIOU loss, $L_{\text{contrastive}}$ is our contrastive matching loss. The comprehensive analysis of each loss component shows in (Sec. 4.3).

3.4. Training hyperparameters

This section specifies the training hyperparameters. We fine-tuned the CYWS change detector [25] using contrastive matching loss and DETR loss [2], leveraging the

pre-trained CYWS model. Transformation estimation followed the method in [26]. The fine-tuning process ran for 200 epochs on four A100 GPUs with a batch size of 16, optimized using the Adam algorithm [16] with a learning rate of 0.0001 and weight decay of 0.0005. The final loss (Eq. (2)) used $\alpha = 3$ and $\beta = 2$. A detailed analysis of hyperparameter selection is provided in (App. C).

4. Hyperparameters Tuning

4.1. Training contrastive matching loss with only ground-truth achieves the highest mAP

We analyze the impact of assigning embeddings from ground-truth boxes or predicted boxes as inputs to the Hungarian algorithm on the matching process (Fig. 3).

Experiments We evaluate three embedding assignment methods for training the contrastive matching loss. The first method assigns embeddings exclusively to predicted bounding boxes. The second method assigns embeddings only to ground-truth bounding boxes. The third method, a hybrid approach, utilizes both ground-truth and predicted bounding boxes, where predicted embeddings are passed to the Hungarian algorithm, and correctly assigned matches replace predicted embeddings with their corresponding ground-truth embeddings, while incorrect assignments retain the original predicted embeddings. In all methods, the output from the Hungarian algorithm is used to compute the contrastive matching loss (Fig. 5).

Results The method relying solely on only ground-truth boxes achieves the highest mean average precision (mAP) across the 🇸🇰, 🇨🇪, and 🇩🇪 datasets. In contrast, combining ground-truth and anticipated boxes results in improved mAP for both the 🇺🇸 and 🇩🇪 datasets. However, due to variations in viewpoint across the 🇸🇰, 🇨🇪, and 🇩🇪 datasets, leveraging predicted boxes for feature embeddings proves insufficient for accurately capturing differences between paired images. Consequently, the mAP is reduced when using predicted boxes alone, compared to using solely ground-truth boxes (Tab. 1).

Model	Predicted	Ground-Truth	🇸🇰	🇺🇸	🇨🇪	🇩🇪	🇩🇪
CYWS [25]			62.73	53.98	76.13	88.97	69.70
Our	✓		69.60	56.08	79.95	89.60	75.43
Our		✓	71.77	57.00	81.07	90.02	78.84
Our	✓	✓	70.86	57.26	79.28	90.44	76.57

Table 1. **Ground-truth** bounding boxes are crucial for training contrastive matching loss effectively. Relying solely on predicted bounding boxes or combining them with ground-truth bounding boxes significantly degrades the model’s **mAP** accuracy.

4.2. Encoder feature maps yield better localization than decoder feature maps

To compute the cost matrix for the Hungarian algorithm in Stage Three, features are extracted from the encoder or decoder in Stage One to generate embeddings for each predicted bounding box (Fig. 3). We hypothesize that using features from different decoder layers allows the extraction of multi-scale information, resulting in embeddings with richer representations compared to those generated solely from the encoder’s output. Specifically, we evaluate features obtained from the output of the encoder’s final layer and the outputs of the first three initial layers of the decoder. **Experiments** In the first experiment, the output from Layer 4.2 of the encoder (ResNet-50) is used, resulting in an embedding of size 2048 being assigned to each predicted bounding box. In the second experiment, the feature volumes from the first three initial layers of the decoder, with dimensions $8 \times 8 \times 4096$, $16 \times 16 \times 2048$, and $32 \times 32 \times 1024$, respectively, are used. We concatenate embedding extracted from three decoder layers to form the final embedding of size 7168 (code).

Results Using the embeddings from the decoder layer does not lead to a better **mAP** score (see Tab. 2) across all datasets. The feature map obtained from the encoder has a higher value of **+0.97** in the 🇸🇰 dataset, **+2.19** in the 🇨🇪 dataset, and **+1.01** in the 🇩🇪 dataset. However, on the 🇺🇸 dataset, it yields a marginal improvement of only **+0.03**. Therefore, we use the **Encoder** feature map for our finetuned model.





Model	Encoder	Decoder	🇸🇰	🇺🇸	🇨🇪	🇩🇪	🇩🇪
Our		✓	70.80	57.03	78.88	89.01	78.58
Our	✓		71.77	57.00	81.07	90.02	78.84

Table 2. Feature embeddings derived from **encoder** feature maps outperform those derived from decoder feature maps on mAP.

4.3. Ablation study of loss function

Our fine-tuning loss (Eq. (2)) has three components: CenterNet loss, DETR loss, and our novel contrastive matching loss. Here, we run an ablation study to show that all three losses contribute to the final result.

Experiments We conduct fine-tuning experiments on the CYWS model under various configurations. In the first setup, we used only the CenterNet loss and DETR loss for training. In our ablation study, we fine-tune the model under different configurations to evaluate the impact of the DETR loss and the Contrastive matching loss on change detection performance. Specifically, we experiment with our model fine-tuned with and without the DETR loss, as well as with and without the Contrastive matching loss. For all these experiments, the models were initialized with weights derived from the pre-trained CYWS model.

Results We find that DETR loss contributes improvements of $+7.02$, $+2.45$, $+2.95$, $+0.79$, $+6.73$ in the , , , **T**,  datasets, respectively, compared to using CenterNet alone. Similarly, the Contrastive matching loss leads to enhancements of $+6.7$, $+3.02$, $+4.94$, $+1.11$, and $+3.49$ across the same datasets, respectively, compared to CenterNet alone. Adding all three losses results in the highest mAP across 4 out of 5 datasets.





Model	CenterNet	DETR	Contrastive				T	
CYWS [25]	✓			62.73	53.98	76.13	88.97	69.70
Our	✓	✓		69.75	56.43	79.08	89.76	76.43
Our	✓		✓	69.43	56.07	79.11	90.08	73.19
Our	✓	✓	✓	71.77	57.00	81.07	90.02	78.84


Table 3. **Loss ablation study.** contrastive matching loss significantly improves mAP score across all datasets, achieving substantial improvements and remaining effective when combined with other losses, such as DETR loss.

5. Results

5.1. Given the same performance on no-change cases, our finetuned detector outperforms state-of-the-art CYWS

Real-world applications require models to perform well in both the change and no-change cases. We test our hypothesis that visual correspondence (*i.e.*, the binary supervision labels of whether two image patches contain a change or not) improves change detection accuracy. We evaluate change detection performance by applying a detection threshold to ensure that the average number of predicted boxes per image in no-change cases remains below 0.01. This is a critical consideration for practical deployment, which has been overlooked in prior work [25].

Experiments We initialize our model with the pre-trained CYWS weights and fine-tune it (Sec. 3.4) using the L_{total} loss function (Eq. (2)). We evaluate mean Average Precision (mAP) on five datasets (Sec. 2.2) using both CYWS [25] and our models. We choose the optimal detection threshold at 0.25 for both models, ensuring the average number of predicted boxes per image in the no-change case remains below **0.01**.

Results Our fine-tuned model outperforms CYWS [25] across all THREE post-processing STAGES (see Tab. 4). Since we keep the fine-tuning strategy fixed and repeat the experiment with various post-processing techniques, we contribute the positive delta in mAP score to our contrastive matching loss (Sec. 3.3). That is, **our contrastive loss improves change detection performance across both change and no-change pairs compared to CYWS [25]**. This performance gap further increases across all five datasets when an optimal threshold is applied. For instance, in the  dataset, the margin increases from $+9.04$

to $+10.97$.


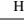
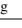
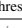



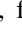
	Model	Det-thres	Align	Hung	Thres				T	
(a)	CYWS				n/a	62.73	53.98	76.13	88.97	69.70
	Our				0.25	71.77	57.00	81.07	90.02	78.84
						$+9.04$	$+3.02$	$+4.94$	$+1.05$	$+9.14$
(b)	CYWS		✓		0.25	51.25	43.40	65.46	86.38	61.68
	Our		✓		0.25	62.22	47.80	71.25	88.08	72.69
						$+10.97$	$+4.40$	$+5.79$	$+1.70$	$+11.01$
(c)	CYWS		✓		0.25	47.83	40.44	64.98	84.76	44.39
	Our		✓	✓	0.25	59.23	44.62	69.23	86.59	58.83
						$+11.40$	$+4.18$	$+4.25$	$+1.83$	$+14.44$
(d)	CYWS		✓	✓	0.25	44.48	39.93	54.16	83.78	44.41
	Our		✓	✓	0.25	56.59	44.67	60.85	85.86	58.88
						$+12.02$	$+5.34$	$+6.69$	$+2.08$	$+14.47$

Table 4. **Change detection (mAP).** The mAP value is calculated using several settings. In this context, we have selected an optimal detection threshold that ensures the average number of predicted boxes per image is below **0.01** on the No-change cases.

Each additional stage, including detection threshold, alignment, and Hungarian matching, contributes to a monotonic reduction in false positives across all five benchmark datasets for both change cases (Tab. 7) and no-change cases. On the  dataset, false positives are reduced by -1.045 . Similar reductions are observed across other datasets: a reduction of -1.474 on the  dataset, -0.216 on , -1.428 on **T**, and -0.059 on  (Tab. 5).

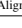
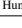
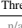


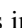
Det-thres	Align	Hung	Thres				T	
				n/a	100	100	100	100
✓			0.1	1.640	1.737	1.372	1.731	0.119
✓			0.1	1.253	1.055	1.219	1.058	0.054
✓		✓	0.1	0.982	0.945	1.309	0.976	0.060
✓	✓	✓	0.1	0.595 (-1.045)	0.263 (-1.474)	1.156 (-0.216)	0.303 (-1.428)	0.060 (-0.059)

Table 5. **Average number of predicted Boxes per image for no change cases (↓).** The effectiveness of applying detection threshold, alignment, and Hungarian in removing false positive predicted box in no change case of the CYWS model. See (Fig. A3) for qualitative examples.

5.2. The alignment stage plays a crucial role in the success of the matching algorithm

Given two sets of boxes of predicted changes [25], our Hungarian-based matching algorithm’s goal is to pair up corresponding changes. The alignment stage (Fig. 3) identifies pairs of corresponding boxes between two images and eliminates boxes that do not have a match. We aim to test the matching accuracy with and without the Alignment stage to understand its importance.

Experiment We repeat our correspondence prediction algorithm (Sec. 3.3) on all five benchmarks with and without the Alignment stage.

Results We find that the Alignment stage plays a crucial role, responsible for $+34.57$ in the  dataset, $+29.27$ in the **T** dataset of CYWS model in matching accuracy. Similarly, in  and **T** datasets, our model’s improvement is $+38.18$ and $+30.04$, respectively (see Tab. 6). See (Fig. A1) for qualitative results.

Model	Det-thres	Align	Hung	Thres				T	
CYWS	✓		✓	0.25	39.72	18.78	56.70	54.73	55.91
CYWS	✓	✓		0.25	38.40	53.22	63.93	83.83	57.59
CYWS	✓	✓	✓	0.25	41.79	53.35 (+34.57)	63.96	84.00 (+29.27)	57.67
Our	✓		✓	0.25	45.77	18.81	63.84	55.27	68.15
Our	✓	✓		0.25	46.00	56.06	68.98	85.22	69.45
Our	✓	✓	✓	0.25	48.35	56.99 (+38.18)	69.72	85.31 (+30.04)	69.53

Table 6. **Alignment** stage contributes to the success of the matching algorithm based on the F1 score. See (Fig. A1) for qualitative examples.

5.3. Contrastive matching loss improves change matching accuracy

The contrastive matching loss directs the model to focus on regions exhibiting changes in both images, filtering out false positives. This approach improves change detection accuracy and boosts the correspondence score relative to the CYWS model.

Experiment We evaluate our model and the CYWS model under three configurations: using a detection threshold, incorporating an alignment stage, and applying the Hungarian algorithm to detect changes across five datasets (Sec. 2.2). The matching score was computed with and without alignment on these datasets.

Model	Det-thres	Align	Hung	Thres				T	
CYWS	✓		✓	0.25	39.72	18.78	56.70	54.73	55.91
Our	✓		✓	0.25	45.77	18.81	63.84	55.27	68.15
					+6.05	+0.03	+7.14	+0.54	+12.24
CYWS	✓	✓		0.25	38.40	53.22	63.93	83.83	57.59
Our	✓	✓		0.25	46.00	56.06	68.98	85.22	69.45
					+7.60	+2.84	+5.05	+1.39	+11.86
CYWS	✓	✓	✓	0.25	41.79	53.35	63.96	84.00	57.67
Our	✓	✓	✓	0.25	48.35	56.99	69.72	85.31	69.53
					+6.56	+3.64	+5.76	+1.31	+11.86

Table 7. **Change correspondence F1 Score.** We examine the matching score in two scenarios—one with alignment and the other without—between our model and CYWS model. Our model performs better than CYWS model in two scenarios. For qualitative examples, see (Fig. A2).

Results Our model, trained with contrastive matching loss, surpasses CYWS across five datasets under both scenarios—with and without alignment. Without alignment, our model yields improvements of +6.05 on , +7.14 on , and +12.24 on . With alignment, it maintains a strong advantage with +6.56 on , +3.64 on , +5.76 on , and +1.31 on T (Tab. 7).

6. Related Work

Change Detection The state-of-the-art model CYWS [25] targets change detection for 2D objects in surveillance images, demonstrating broad applicability without retraining. To extend this capability to 3D objects, CYWS-3D [26] was proposed. However, neither approach identifies corresponding changes between image pairs.

Methods like Changemamba [4], SCanNet [5], and STADE-CDNet [19] are specifically designed for remote sensing applications. In this domain, images generally exhibit a single change between two images, simplifying the correspondence problem. In contrast, our approach addresses a more complex correspondence problem, involving multiple changes between two surveillance images (see Fig. A4b).

Change Segmentation Prior research, including [1, 28], has focused on detecting changes in street views, while studies such as [9, 27, 35, 37, 38] concentrate on satellite imagery. [40] presents a novel zero-shot change segmentation approach specifically for satellite images. Similarly, our model demonstrates strong performance across four zero-shot benchmarks.

Change Captioning The Spot-the-Diff () change captioning dataset, introduced by [13], contains 13,000 image pairs captured from surveillance cameras. Research in this domain also explores remote sensing image datasets [3] and addresses challenges in datasets such as CLEVR-Change, CLEVR-DC, and Bird-to-Words [8, 10–12, 15, 21, 30, 39], which either simulate or capture real-world changes. These works lack effective change localization, and change captioning becomes more complex when multiple changes occur between two images. Our approach addresses these issues by providing change localization with correspondence, simplifying interpretation. [32] presents STVChrono, a benchmark dataset of 71,900 Google Street View images from 18 years across 50 cities to study long-term changes in outdoor scenes. However, its creation is labor-intensive and time-consuming, limiting scalability. In contrast, our dataset can be efficiently scaled with a simple process.

7. Discussion and Conclusions

Limitations We observe that the accuracy of Point estimation (Stage 2 in our pipeline) plays a critical role in our pipeline. Specifically, images with significant distortions or detailed textures (see Fig. A4a) poses a challenge to Point Estimate to align two images and leads to estimation accuracy declines, impacting alignment stage effectiveness.

Conclusions This study proposes a novel contrastive matching loss function that improves detector accuracy and matching accuracy, surpassing the CYWS method. The post-processing algorithm ensures accurate pairing of changes, and a new metric is introduced for evaluating matching scores across models.

Acknowledgement

We thank Thang Pham, Ali Yildirim, Giang Nguyen, and Tin Nguyen at Auburn University for feedback and discussions of the earlier results. AN was supported by the NSF Grant No. 1850117 & 2145767, and donations from Naph-Care Foundation & Adobe Research.

References

- [1] Pablo F Alcantarilla, Simon Stent, German Ros, Roberto Arroyo, and Riccardo Gherardi. Street-view change detection with deconvolutional networks. *Autonomous Robots*, 42:1301–1322, 2018. [8](#)
- [2] Nicolas Carion, Francisco Massa, Gabriel Synnaeve, Nicolas Usunier, Alexander Kirillov, and Sergey Zagoruyko. End-to-end object detection with transformers. In *European conference on computer vision*, pages 213–229. Springer, 2020. [2](#), [5](#)
- [3] Shizhen Chang and Pedram Ghamisi. Changes to captions: An attentive network for remote sensing change captioning. *arXiv preprint arXiv:2304.01091*, 2023. [8](#)
- [4] Hongruixuan Chen, Jian Song, Chengxi Han, Junshi Xia, and Naoto Yokoya. Changemamba: Remote sensing change detection with spatio-temporal state space model. *arXiv preprint arXiv:2404.03425*, 2024. [8](#)
- [5] Lei Ding, Jing Zhang, Haitao Guo, Kai Zhang, Bing Liu, and Lorenzo Bruzzone. Joint spatio-temporal modeling for semantic change detection in remote sensing images. *IEEE Transactions on Geoscience and Remote Sensing*, 2024. [8](#)
- [6] Mengjin Dong, Long Xie, Sandhitsu R Das, Jiancong Wang, Laura EM Wisse, Robin DeFlores, David A Wolk, Paul A Yushkevich, Alzheimer’s Disease Neuroimaging Initiative, et al. Deepatrophy: Teaching a neural network to detect progressive changes in longitudinal mri of the hippocampal region in alzheimer’s disease. *Neuroimage*, 243:118514, 2021. [1](#)
- [7] Kaiwen Duan, Song Bai, Lingxi Xie, Honggang Qi, Qingming Huang, and Qi Tian. Centernet: Keypoint triplets for object detection. In *Proceedings of the IEEE/CVF international conference on computer vision*, pages 6569–6578, 2019. [3](#), [4](#), [5](#)
- [8] Maxwell Forbes, Christine Kaeser-Chen, Piyush Sharma, and Serge Belongie. Neural naturalist: generating fine-grained image comparisons. *arXiv preprint arXiv:1909.04101*, 2019. [8](#)
- [9] Maoguo Gong, Tao Zhan, Puzhao Zhang, and Qiguang Miao. Superpixel-based difference representation learning for change detection in multispectral remote sensing images. *IEEE Transactions on Geoscience and Remote sensing*, 55(5):2658–2673, 2017. [8](#)
- [10] Zixin Guo, Tzu-Jui Julius Wang, and Jorma Laaksonen. Clip4idc: Clip for image difference captioning. *arXiv preprint arXiv:2206.00629*, 2022. [8](#)
- [11] Mehrdad Hosseinzadeh and Yang Wang. Image change captioning by learning from an auxiliary task. In *Proceedings of the IEEE/CVF Conference on Computer Vision and Pattern Recognition*, pages 2725–2734, 2021. [8](#)
- [12] Qingbao Huang, Yu Liang, Jielong Wei, Yi Cai, Hanyu Liang, Ho-fung Leung, and Qing Li. Image difference captioning with instance-level fine-grained feature representation. *IEEE transactions on multimedia*, 24:2004–2017, 2021. [8](#)
- [13] Harsh Jhamtani and Taylor Berg-Kirkpatrick. Learning to describe differences between pairs of similar images. *arXiv preprint arXiv:1808.10584*, 2018. [1](#), [2](#), [8](#)
- [14] Qirui Jiao, Daoyuan Chen, Yilun Huang, Yaliang Li, and Ying Shen. Img-diff: Contrastive data synthesis for multimodal large language models. *arXiv preprint arXiv:2408.04594*, 2024. [2](#)
- [15] Hoeseong Kim, Jongseok Kim, Hyungseok Lee, Hyunsung Park, and Gunhee Kim. Agnostic change captioning with cycle consistency. In *Proceedings of the IEEE/CVF International Conference on Computer Vision*, pages 2095–2104, 2021. [8](#)
- [16] Diederik P Kingma and Jimmy Ba. Adam: A method for stochastic optimization. *arXiv preprint arXiv:1412.6980*, 2014. [6](#)
- [17] Harold W Kuhn. The hungarian method for the assignment problem. *Naval research logistics quarterly*, 2(1-2):83–97, 1955. [2](#)
- [18] Alina Kuznetsova, Hassan Rom, Neil Alldrin, Jasper R. R. Uijlings, Ivan Krasin, Jordi Pont-Tuset, Shahab Kamali, Stefan Popov, Matteo Mallocci, Tom Duerig, and Vittorio Ferrari. The open images dataset V4: unified image classification, object detection, and visual relationship detection at scale. *CoRR*, abs/1811.00982, 2018. [2](#)
- [19] Zhi Li, Siying Cao, Jiakun Deng, Fengyi Wu, Ruilan Wang, Junhai Luo, and Zhenming Peng. Stade-cdnet: Spatial-temporal attention with difference enhancement-based network for remote sensing image change detection. *IEEE Transactions on Geoscience and Remote Sensing*, 62:1–17, 2024. [8](#)
- [20] R. Padilla, S. L. Netto, and E. A. B. da Silva. A survey on performance metrics for object-detection algorithms. In *2020 International Conference on Systems, Signals and Image Processing (IWSSIP)*, pages 237–242, 2020. [3](#)
- [21] Dong Huk Park, Trevor Darrell, and Anna Rohrbach. Robust change captioning. In *Proceedings of the IEEE/CVF International Conference on Computer Vision*, pages 4624–4633, 2019. [8](#)
- [22] Julia Patriarche and Bradley Erickson. A review of the automated detection of change in serial imaging studies of the brain. *Journal of digital imaging*, 17:158–174, 2004. [1](#)
- [23] Hai Phan and Anh Nguyen. Deepface-emd: Re-ranking using patch-wise earth mover’s distance improves out-of-distribution face identification. In *Proceedings of the IEEE/CVF Conference on Computer Vision and Pattern Recognition*, pages 20259–20269, 2022. [5](#)
- [24] Abhijit Guha Roy, Nassir Navab, and Christian Wachinger. Concurrent spatial and channel ‘squeeze & excitation’ in fully convolutional networks. In *Medical Image Computing and Computer Assisted Intervention–MICCAI 2018: 21st International Conference, Granada, Spain, September 16-20, 2018, Proceedings, Part I*, pages 421–429. Springer, 2018. [4](#)
- [25] Ragav Sachdeva and Andrew Zisserman. The change you want to see. In *Proceedings of the IEEE/CVF Winter Conference on Applications of Computer Vision*, pages 3993–4002, 2023. [1](#), [2](#), [3](#), [5](#), [6](#), [7](#), [8](#), [13](#)
- [26] Ragav Sachdeva and Andrew Zisserman. The change you want to see (now in 3d). In *Proceedings of the IEEE/CVF International Conference on Computer Vision*, pages 2060–2069, 2023. [1](#), [2](#), [3](#), [6](#), [8](#)

- [27] Sudipan Saha, Francesca Bovolo, and Lorenzo Bruzzone. Unsupervised deep change vector analysis for multiple-change detection in vhr images. *IEEE Transactions on Geoscience and Remote Sensing*, 57(6):3677–3693, 2019. 8
- [28] Ken Sakurada and Takayuki Okatani. Change detection from a street image pair using cnn features and superpixel segmentation. In *British Machine Vision Conference*, 2015. 8
- [29] Paul-Edouard Sarlin, Daniel DeTone, Tomasz Malisiewicz, and Andrew Rabinovich. Superglue: Learning feature matching with graph neural networks. In *Proceedings of the IEEE/CVF conference on computer vision and pattern recognition*, pages 4938–4947, 2020. 4
- [30] Xiangxi Shi, Xu Yang, Jiuxiang Gu, Shafiq Joty, and Jianfei Cai. Finding it at another side: A viewpoint-adapted matching encoder for change captioning. In *Computer Vision–ECCV 2020: 16th European Conference, Glasgow, UK, August 23–28, 2020, Proceedings, Part XIV 16*, pages 574–590. Springer, 2020. 8
- [31] Simon Stent, Riccardo Gherardi, Björn Stenger, and Roberto Cipolla. Detecting change for multi-view, long-term surface inspection. In *BMVC*, pages 127–1, 2015. 1
- [32] Yanjun Sun, Yue Qiu, Mariia Khan, Fumiya Matsuzawa, and Kenji Iwata. The stvchrono dataset: Towards continuous change recognition in time. In *Proceedings of the IEEE/CVF Conference on Computer Vision and Pattern Recognition*, pages 14111–14120, 2024. 8
- [33] Roman Suvorov, Elizaveta Logacheva, Anton Mashikhin, Anastasia Remizova, Arsenii Ashukha, Aleksei Silvestrov, Naejin Kong, Harshith Goka, Kiwoong Park, and Victor Lempitsky. Resolution-robust large mask inpainting with fourier convolutions. In *Proceedings of the IEEE conference on computer vision and pattern recognition*, 2021. 2
- [34] Hao Tan, Franck Dernoncourt, Zhe Lin, Trung Bui, and Mohit Bansal. Expressing visual relationships via language. In Anna Korhonen, David Traum, and Lluís Màrquez, editors, *Proceedings of the 57th Annual Meeting of the Association for Computational Linguistics*, pages 1873–1883, Florence, Italy, July 2019. Association for Computational Linguistics. 1
- [35] Congcong Wang, Wenbin Sun, Deqin Fan, Xiaoding Liu, and Zhi Zhang. Adaptive feature weighted fusion nested u-net with discrete wavelet transform for change detection of high-resolution remote sensing images. *Remote Sensing*, 13(24):4971, 2021. 8
- [36] Junhui Wu, Yun Ye, Yu Chen, and Zhi Weng. Spot the difference by object detection. *arXiv preprint arXiv:1801.01051*, 2018. 1
- [37] Quanfu Xu, Keming Chen, Guangyao Zhou, and Xian Sun. Change capsule network for optical remote sensing image change detection. *Remote Sensing*, 13(14):2646, 2021. 1, 8
- [38] Le Yang, Yiming Chen, Shiji Song, Fan Li, and Gao Huang. Deep siamese networks based change detection with remote sensing images. *Remote Sensing*, 13(17):3394, 2021. 8
- [39] Linli Yao, Weiyang Wang, and Qin Jin. Image difference captioning with pre-training and contrastive learning. In *Proceedings of the AAAI Conference on Artificial Intelligence*, volume 36, pages 3108–3116, 2022. 8
- [40] Zhuo Zheng, Yanfei Zhong, Liangpei Zhang, and Stefano Ermon. Segment any change. *arXiv preprint arXiv:2402.01188*, 2024. 1, 2, 8

Appendix for: Improving Zero-Shot Object-Level Change Detection by Incorporating Visual Correspondence

A. Upper bound accuracy of correspondence algorithm

Here, we want to estimate the correspondence component. Correspondence algorithm consists of alignment step before using the Hungarian algorithm. By using ground-truth boxes, we can evaluate the maximum accuracy of the matching algorithm.

Experiments To assess the effectiveness of the post-processing method we employ ground-truth boxes directly rather than utilising the change detector’s projected box output as the feature extractor’s input.

Results The findings presented in Tab. A1 upper bound indicate that our matching method demonstrates strong performance in F_1 score when applied to both the 🗨️(+100) and T(+99.96) algorithms. A gap persists in the availability of the 🗨️(96.50) and 🗨️(91.68) datasets. The efficacy of the transformation matrix is limited in certain challenging scenarios involving 🗨️ or 🗨️. The 🗨️ dataset contains numerous artifacts, which hinder the accurate estimation of the transformation matrix.

Change (F1 Score)					
Model	🗨️	🗨️	🗨️	T	🗨️
Ground-truth Baseline	91.68	100	96.50	99.96	99.94

Table A1. **Correspondence Accuracy Upper Bound.** Using ground truth boxes as input for matching algorithm

B. Features of mean pooling provide more accurate correspondence than cropped images features

The proposed approach offers flexibility in selecting methods for assigning embeddings to predicted boxes. This section evaluates two methodologies for generating embeddings. To identify the optimal method, we conduct a comparative analysis using our fine-tuned model. The effectiveness of each approach is assessed based on the matching score (F1).

Experiments This section analyzes the impact of two embedding assignment methods: mean-pooling and region cropping on the correspondence score. The analysis is conducted based on the methodologies outlined in (Sec. 3.3).

Results We hypothesize that using only cropped images reduces the availability of contextual information surrounding the object, resulting in lower correspondence accuracy. The average feature method consistently outperforms the cropping method across all five datasets, with significant improvements observed in the T and 🗨️ datasets. Consequently, we have adopted the average feature technique for all subsequent experiments. Detailed results are presented in Tab. A2.

Model	Average	Crop	Thres	🗨️	🗨️	🗨️	T	🗨️
Our + ResNet-50		✓	0.25	44.10	56.29	68.10	67.73	62.25
Our + ResNet-50	✓		0.25	46.19	56.94	69.52	85.33	69.53
				+2.09	+0.65	+1.42	+17.60	+7.28

Table A2. Features obtained using the **average** method achieve higher F1 scores compared to those derived from the cropping method. This approach consistently produces reliable results across all datasets, with particularly notable performance on the T and 🗨️ datasets.

C. Training hyperparameters

Results We follow the training hyperparameters in (Sec. 3.4). We investigate the impact of training parameters, including the number of epochs and learning rate, on model performance. Training for 500 epochs led to overfitting, reducing zero-shot accuracy on the 🗨️, 🌐, T, and 📄 datasets (Tab. A4). Increasing the learning rate from 0.0001 to 0.0005 further degraded accuracy (Tab. A3). Additionally, using a deeper decoder did not improve accuracy (Tab. A5).


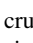
Change (mAP Score)									
Model	LR	CenterNet	DETR	Contrastive	🗨️	🗨️	🌐	T	📄
Our	0.0005	✓	✓	✓	57.87	47.95	68.20	88.54	60.33
Our	0.0001	✓	✓	✓	71.77	57.00	81.07	90.02	78.84

Table A3. **Training with different learning rate (LR).** Using different learning rate in training

Change (mAP Score)									
Model	Epochs	CenterNet	DETR	Contrastive	🗨️	🗨️	🌐	T	📄
Our	500	✓	✓	✓	72.15	54.17	78.64	89.01	78.65
Our	200	✓	✓	✓	71.77	57.00	81.07	90.02	78.84

Table A4. **Training with more epochs.** Training the model for 500 epochs decreases accuracy in zero-shot testing on the 🗨️, 🌐, T, and 📄 datasets.



Figure A1. With the significant improvement in the  and  datasets, the alignment stage is a crucial component in increasing correspondence accuracy. The second row’s findings demonstrate how the alignment step aids in correcting every case’s incorrect matching in the first row. You may view the improvement’s specifics in the Tab. 6.

D. Training with a deeper decoder does not enhance model accuracy

In order to find the best change detection architecture, we added more layers to the decoder in this section.

Experiment We used [256, 128, 64] channels for each decoder layer in the prior configuration. We add two further layers with 32 and 8 channels, respectively, in this configuration.

Results The outcomes of employing deeper decoder layers are displayed in Tab. A5. The findings demonstrate that the final accuracy decreases with the number of decoder layers.






		Change (mAP Score)							
Model	Epochs	CenterNet	DETR	Contrastive					
Our	200	✓	✓	✓	51.76	49.70	63.95	87.57	54.39
Our	200	✓	✓	✓	71.77	57.00	81.07	90.02	78.84

Table A5. **Training with a deeper decoder** does not enhance model accuracy

E. The alignment stage plays a crucial role in the success of the matching algorithm

The qualitative results Fig. A1 we present in this section demonstrate how well our alignment stage worked to enhance the matched pairs of modifications displayed in the Tab. 6.

F. Correspondence

We present qualitative results in this part that contrast our model with CYWS model in terms of matching qualitative. According to the qualitative results, our model outperforms CYWS model in the matching score, as indicated by the Tab. 7. See qualitative results in Fig. A2

G. Reduce false positive predicted box in no-change case

The output from CYWS model in the default situations is shown in the first row of Fig. A3. The outcomes of our post-processing procedure are shown in the row that follows.

H. Additional qualitative results

In this part, we present further qualitative comparison findings between our fine-tuned model and CYWS [25] model following the use of a detection threshold of 0.25 and a post-processing technique. CYWS findings are shown in the first row, while the results of our model are shown in the second row. For qualitative results, see Fig. A4.

I. Number of predicted box after applying detection threshold

For both the ground-truth and our refined model with different thresholds, CYWS, we display the average number of boxes per image. You can view the detail in the Tab. A6

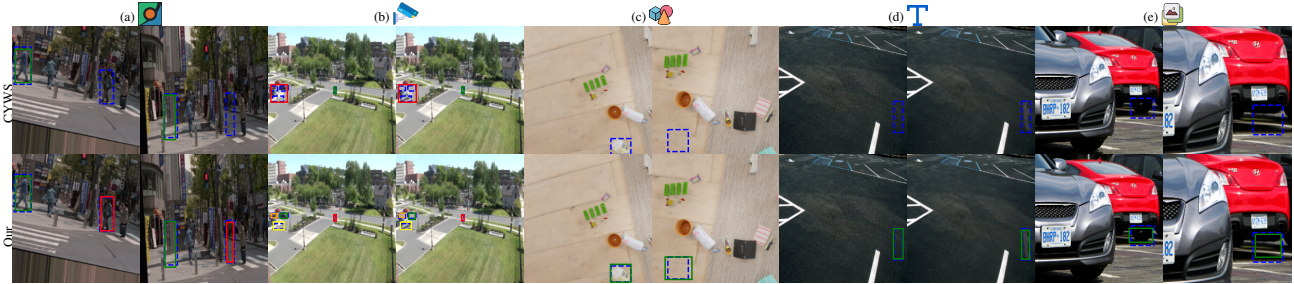


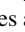
Figure A2. CYWS model, as seen in (a), (b), (c), (d) and (e), is unable to identify every difference between two images. Conversely, our model is able to identify every change in the two images. CYWS model can only identify one change for the entire region in the  example, where three changes appear at nearly the same location. Our model, on the other hand, can identify each of the three changes independently. We hypothesise that the model learns the number of changes implicitly based on information gleaned from the contrastive matching loss. Check Tab. 7 for quantitative results.



Figure A3. In no-change scenarios, our post-processing approach reduces false positive predicted boxes.





		Change				
		Avg Predicted Box Per Image				
Model	Thres				T	
Ground-Truth	n/a	1.93	5.85	1.80	1.10	1.0
CYWS	n/a	100	100	100	100	100
Our	n/a	100	100	100	100	100
CYWS	0.1	3.63	6.55	2.27	2.55	3.54
Our	0.1	3.21	7.23	2.37	2.25	2.64
CYWS	0.2	1.75	4.38	1.95	1.23	1.17
Our	0.2	1.85	4.90	1.96	1.19	1.14
CYWS	0.3	0.98	2.81	1.75	0.80	0.54
Our	0.3	1.20	3.13	1.79	0.84	0.67
CYWS	0.4	0.55	1.38	1.50	0.49	0.26
Our	0.4	0.70	1.48	1.56	0.63	0.37
CYWS	0.5	0.29	0.59	1.08	0.42	0.10
Our	0.5	0.45	0.60	1.18	0.44	0.18

Table A6. **Average Predicted Box Per Image for Change with Different Thresholds.** Evaluate the influence of detection threshold on the number of predicted boxes per image in change case with CYWS model and our finetuned model

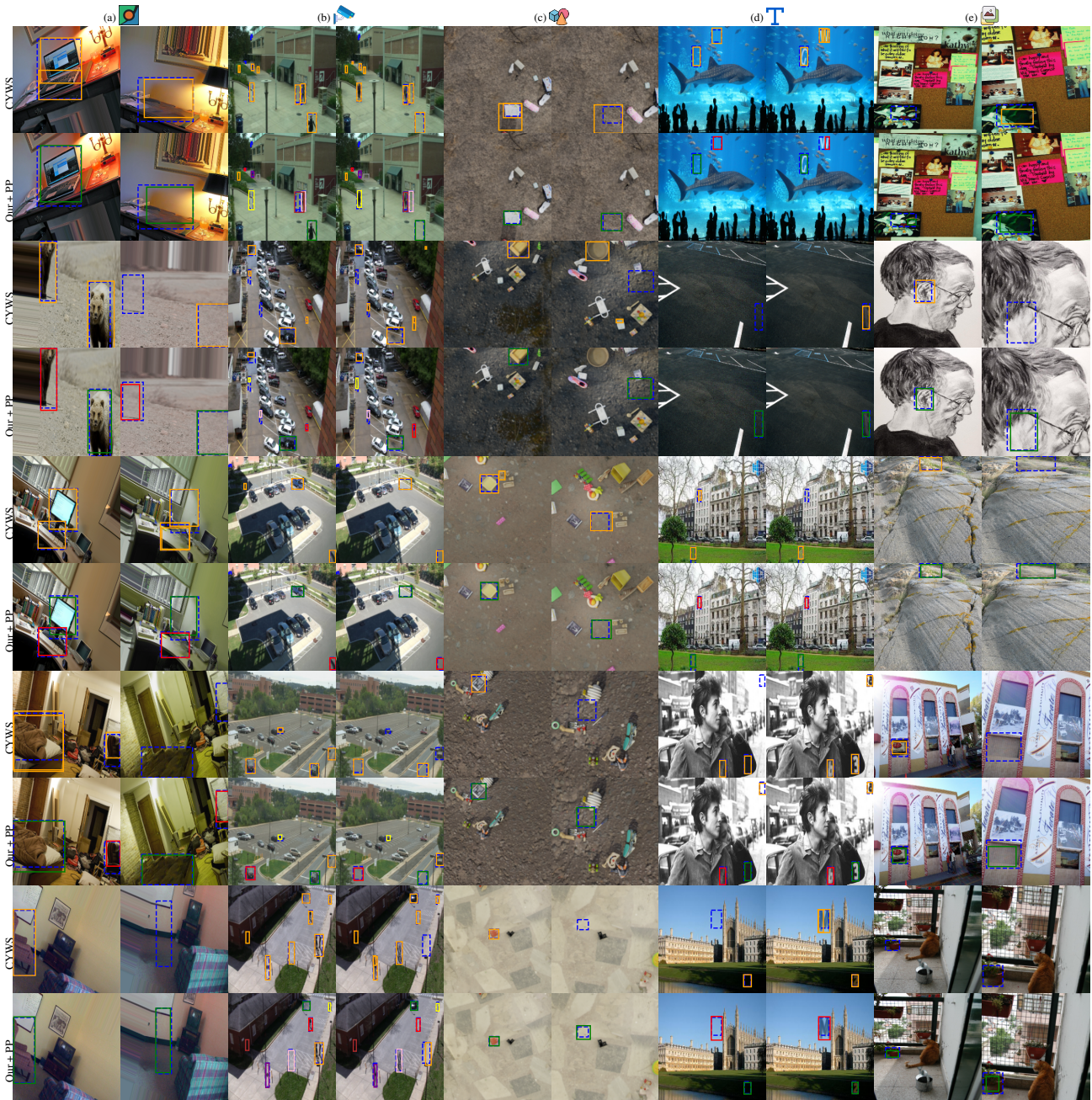







Figure A4. When comparing our model’s change detection output to that of CYWS model, it is evident that our contrastive matching loss enhances the model’s accuracy. Additionally, our post-processing technique can apply in many situations with multiple modifications



Figure A5. Contrasting the results following change detection and using our post-processing both with and without the alignment step. Evaluation of the findings in , , , , and  demonstrates the significance of the alignment stage